Available online at www.sciencedirect.com

SciVerse ScienceDirect

Magnetic Resonance Imaging 30 (2012) 471–484

MAGNETIC RESONANCE IMAGING

Measurement and characterization of the human spinal cord SEEP response using event-related spinal fMRI☆

Chase R. Figley[a,1], Patrick W. Stroman[a,b,c,*]

[a]Centre for Neuroscience Studies, Queen's University, Kingston, Ontario, Canada
[b]Department of Diagnostic Radiology, Queen's University, Kingston, Ontario, Canada
[c]Department of Physics, Queen's University, Kingston, Ontario, Canada

Received 21 July 2011; revised 14 October 2011; accepted 4 December 2011

Abstract

Although event-related fMRI is able to reliably detect brief changes in brain activity and is now widely used throughout systems and cognitive neuroscience, there have been no previous reports of event-related spinal cord fMRI. This is likely attributable to the various technical challenges associated with spinal fMRI (e.g., imaging a suitable length of the cord, reducing image artifacts from the vertebrae and intervertebral discs, and dealing with physiological noise from spinal cord motion). However, with many of these issues now resolved, the largest remaining impediment for event-related spinal fMRI is a deprived understanding of the spinal cord fMRI signal time course. Therefore, in this study, we used a proton density-weighted HASTE sequence, with functional contrast based on signal enhancement by extravascular water protons (SEEP), and a motion-compensating GLM analysis to (i) characterize the SEEP response function in the human cervical spinal cord and (ii) demonstrate the feasibility of event-related spinal fMRI. This was achieved by applying very brief (1 s) epochs of 22°C thermal stimulation to the palm of the hand and measuring the impulse response function. Our results suggest that the spinal cord SEEP response (time to peak ≈8 s; FWHM ≈4 s; and probably lacking pre- and poststimulus undershoots) is slower than previous estimates of SEEP or BOLD responses in the brain, but faster than previously reported spinal cord BOLD responses. Finally, by detecting and mapping consistent signal-intensity changes within and across subjects, and validating these regions with a block-designed experiment, this study represents the first successful demonstration of event-related spinal fMRI.

Keywords: Event-related; fMRI; Human; Impulse response; RESPITE; Response function; SEEP; Spinal cord; Thermal stimulation

1. Introduction

Event-related functional magnetic resonance imaging (fMRI) is now commonly used throughout systems and cognitive neuroscience to measure changes in neural activity in response to brief cognitive or sensory-motor tasks [1,2]. This method expands the utility of fMRI by allowing researchers to investigate faster and more biologically relevant tasks/stimuli than traditional block-designed studies and permits simultaneous evaluations of multiple stimuli within the same fMRI session. This property can be exploited to investigate how the nervous system responds to different types of stimuli or "oddball" tasks [3], variations in presentation order [4], as well as responses to error trials [5]. However, because there are only a small number of groups using fMRI to study the spinal cord and there are many technical challenges associated with doing so [6–9], there have been no successful reports of event-related spinal fMRI in the literature to date. In order to deal with these challenges, spinal fMRI data are typically acquired with different parameters than conventional brain fMRI, and while there is somewhat of a methodological divide between groups still

☆ Grant support: International Spinal Research Trust (U.K.), Canada Research Chairs Program, Canadian Institutes of Health Research Canada Graduate Scholarships Program and the Queen's University Centre for Neuroscience Studies.

* Corresponding author. Department of Diagnostic Radiology and Physics, c/o Centre for Neuroscience Studies, Queen's University, Kingston, Ontario, Canada K7L 3N6. Tel.: +1 613 533 3245; fax: +1 613 533 6840.
E-mail address: stromanp@queensu.ca (P.W. Stroman).
[1] Current address: Department of Psychological and Brain Sciences and Solomon H. Snyder Department of Neuroscience, Johns Hopkins University, Baltimore, MD, USA.

0730-725X/$ – see front matter © 2012 Elsevier Inc. All rights reserved.
doi:10.1016/j.mri.2011.12.015

using conventional T_2^*-weighted gradient-echo echo-planar-imaging (GE-EPI) and those favoring PD-weighted turbo spin-echo (TSE) imaging, previous reports have shown that magnetic susceptibility artifacts from the vertebrae and intervertebral discs can be largely overcome using the latter [10,11]. Moreover, TSE methods are thought to be more robust to respiration-induced magnetic field perturbations because of their inherent resiliency to magnetic susceptibility changes and the spinal cord's close proximity to the lungs [8,12]. However, the choice of acquisition parameters also affects the physiological basis of the observed functional contrast. While T_2- and T_2^*-weighted parameters are sensitive to blood oxygen level-dependent (BOLD) contrast, resulting from hemodynamic changes and alterations in oxy/deoxyhemoglobin concentration [13–15], PD-weighted fMRI methods are sensitive to signal enhancement by extravascular water protons (SEEP), which has been attributed to cell swelling and tissue water content changes in regions of synaptic activity [16–19].

By measuring the time courses of SEEP and BOLD changes in the brain, it has been shown that the two mechanisms also have different response characteristics. In the brain, the peak of the SEEP response appears to lag corresponding BOLD changes by approximately 1 s, and the return to baseline occurs more slowly with no poststimulus undershoot [20]. However, despite the fact that TSE parameters and SEEP contrast have now been employed in a number of block-designed spinal fMRI studies, the spinal cord SEEP response has not yet been well characterized. Instead, the experimental paradigms in these studies have typically been convolved with the brain-derived SEEP response [20], assuming a similar signal time course for the brain and spinal cord. However, while this assumption is probably valid for block-designed paradigms with long periods of rest and activation, accurately modeling the temporal characteristics of the response is critically important for event-related fMRI analysis. For example, modeling data have shown that, while small differences between estimated and true fMRI responses have less impact on the sensitivity of event-related fMRI at the single subject level, temporal mismatches as small as 1 s can significantly increase the occurrence of false negatives in group analyses [21]. Therefore, characterizing the spinal cord SEEP response and confirming its consistency across subjects are both critical steps that must be achieved before PD-weighted, TSE spinal fMRI can be used to study event-related paradigms.

Several studies have shown that the amplitude and timing of BOLD signals differ across cortical areas [21,22], suggesting that the large neuroanatomical (cytoarchitectural and vascular) differences between the brain and spinal cord may lead to even more significant variations in the BOLD response. This has been supported by a recent study [23] showing that the spinal cord BOLD signal (i) does not peak until approximately 9 s (i.e., much later than the canonical brain response), (ii) has a relatively wide response curve and (iii) has little or no poststimulus undershoot. In light of these substantial regional differences, we sought to determine whether there were equally large discrepancies between brain and spinal cord SEEP signals. However, it is important to point out that owing to the mechanistic differences between BOLD and SEEP contrasts [16–18] and their different response characteristics in the brain, it does not necessarily follow that the spinal cord SEEP response will parallel the spinal cord BOLD response.

Finally, the sensitivity and specificity of PD-weighted TSE spinal fMRI have recently been improved with the advent of a motion-compensating general linear model (GLM) analysis [24], which uses retrospective spinal cord motion time-course estimates (RESPITE) to reduce the effects of cardiac-related spinal cord motion [25–27]. Therefore, the purpose of the present study was to exploit the improved sensitivity of these motion-compensating spinal fMRI techniques to measure the signal intensity changes elicited by brief periods of cold thermal stimulation and, for the first time, characterize the SEEP response function in the human spinal cord *and* demonstrate the feasibility of event-related spinal fMRI.

2. Materials and methods

2.1. Test subjects

Data were obtained from 10 healthy volunteers (5 male; 5 female) with no history or evidence of spinal cord or vertebral injury/dysmorphology. Subject age, weight and height ranged from 18 to 22 years (mean±SD = 20±2), 53 to 91 kg (mean±SD = 67±11) and 1.60 to 1.83 m (mean±SD = 1.71±0.06), respectively. All volunteers provided informed consent before partaking in the study, which had received prior approval from the institutional research ethics board.

2.2. Data acquisition

All image data were acquired on a 3 T Siemens Magnetom Tim Trio (Erlangen, Germany) using a body coil to transmit the radiofrequency excitation pulses and a 12-channel phased array (receive-only) posterior spine coil to detect the MR signal. Subjects were positioned supine and carefully aligned on the scanner bed using a bore-mounted laser guide. A wireless pulse oximeter was placed on each subject's left index finger to record the peripheral pulse throughout each experiment. Initially, three-plane and coronal localizer images of the spine and spinal cord were acquired to provide a 3D position reference for subsequent slice alignment.

Imaging parameters for the time-series fMRI data were based on previously reported protocols for optimal SEEP contrast at 3 T [11,28,29]. The method employed a half-Fourier acquisition turbo spin-echo (HASTE) pulse sequence with nine contiguous sagittal slices; TE=minimum (38 ms);

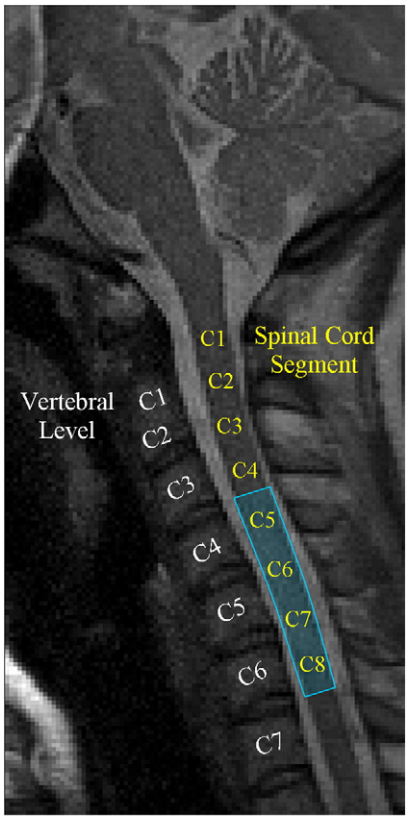

Fig. 1. Representative mid-sagittal image from a spinal fMRI dataset based on SEEP contrast. Predominantly proton density-weighted images were acquired with a HASTE pulse sequence (TE=38 ms; TR=9 s; FOV=200×100 mm^2; voxel volume=1.02×1.02×2.00 mm^3), yielding optimal SEEP contrast and distortion-free images throughout the cervical spinal cord and brainstem. Also denoted are the vertebral levels (white text), spinal cord segments (yellow text) and the C5–C8 anatomical spinal cord mask from which the activity masks were extracted (blue).

TR=9 s (1000 ms/slice); field of view (FOV)=200×100 mm^2 spanning the entire cervical spinal cord, brainstem and thalamus; flip angle=90° with 150° refocusing pulses; slice thickness=2.00 mm; in-plane resolution=1.02×1.02 mm^2. Spatial saturation bands were applied anterior to the spine to eliminate signal from the heart and lungs, and flow compensation gradients were applied in the rostral–caudal direction to minimize cerebrospinal fluid flow artifacts. As shown in Fig. 1, this method provides complete coverage of the cervical spinal cord and brainstem with adequate signal-to-noise ratio and excellent spatial resolution (2.08 mm^3), to minimize partial volume effects.

2.3. Experimental design

2.3.1. General

After the initial setup and acquisition of localizer images, four spinal fMRI sessions (one block-designed and three event-related) were acquired for each subject, as outlined below.

2.3.2. Block-designed spinal fMRI protocol

An initial block-designed paradigm was used to investigate the effects of 22°C cold thermal stimulation applied to the palm of the right hand. All thermal stimuli were delivered with a Medoc TSA-II thermal sensory analyzer (Medoc, Ramat Yihai, Israel) with a 3×3-cm thermal probe placed on the right thenar eminence, corresponding approximately to the C6 dermatome [30,31]. For the block-designed experiment, four 63-s (7 volume) epochs of 32°C (i.e., skin temperature) baseline conditions were interleaved with three 45-s (5 volume) epochs of 22°C cold thermal stimulation. Three prescan volumes were acquired before the initial baseline period to allow the transverse magnetization to achieve a steady state. Therefore, including the spin-preparation volumes, the total block-designed experiment consisted of 46 volumes (total acquisition time of 6.9 min).

2.3.3. Event-related spinal fMRI protocol

To establish the time course of the SEEP impulse response function, spinal fMRI data were acquired during a slow event-related paradigm of brief, evenly spaced applications of 22°C cold thermal stimulation. The imaging parameters, equipment and thermode placement were the same as the block-designed experiment (described above). The slow event-related paradigm consisted of 1-s epochs of constant 22°C thermal stimulation and 25-s baseline periods of 32°C, with cooling and heating ramps set to the limits of the stimulus delivery system (i.e., ±10°C/s), taking 1 s to ramp down to 22°C and another 1 s to ramp back to the 32°C baseline. The total peak-to-peak interstimulus interval (ISI) was 28 s, allowing the SEEP response to increase and return to baseline between sequential applications of thermal stimulation.

The fixed relation between our thermal paradigm and the image acquisition timing (TR=9 s) produced a discrete sampling of the peristimulus response that was unique for each of the nine slices in the imaging volume. As shown in Fig. 2A, three or four unique phases of the SEEP response (depending on the slice acquisition timing) were measured following each stimulus event. Therefore, by acquiring different peristimulus times over a series of stimuli, as previously described [32], the SEEP response was able to be fully sampled over the course of 28 volumes (252 s) with high temporal resolution (1 Hz) relative to the 9-s repetition time. Because each event-related protocol acquired a total of 56 volumes (plus the spin-preparation volumes), the complete SEEP response was measured exactly twice per event-related session (total acquisition time of 8.7 min).

In addition to the first session, each subject subsequently completed the event-related experiment two more times, so that the entire SEEP impulse response was sampled six times over the course of three consecutive event-related sessions. Short breaks were taken between sessions to permit quality assurance checks, and in the event of subject motion, the session was discarded and reacquired (with corrected slice alignment/positioning if necessary).

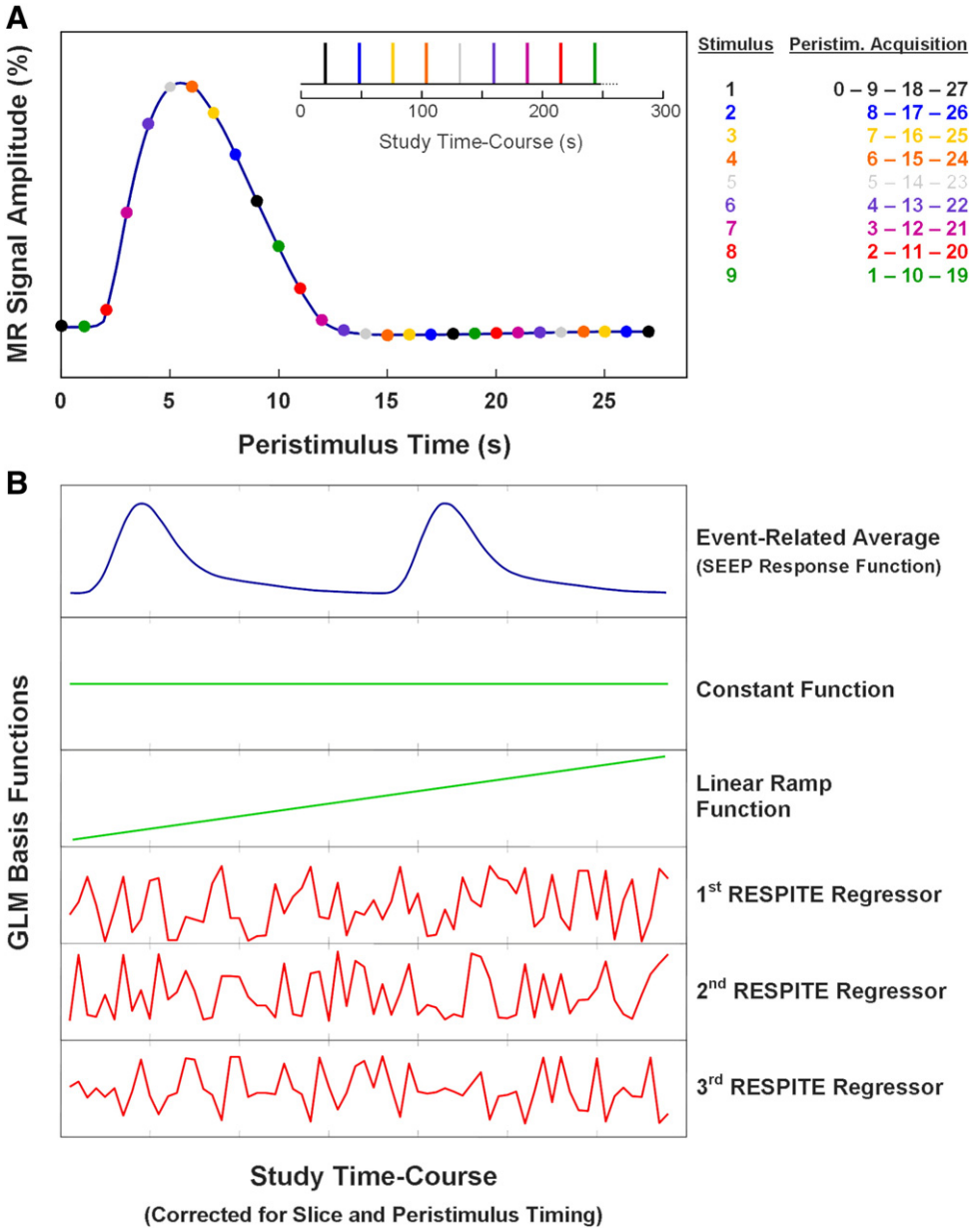

Fig. 2. Event-related spinal fMRI data acquisition and analysis. (A) The peristimulus time courses, for all nine slices in the imaging volume, were measured over the course of nine stimuli by sampling 28 phases of the SEEP response at a rate of 1 Hz. Because 18 stimuli were presented, two entire responses were acquired in each event-related session. (B) After time-locking the responses to the stimuli, event-related data were analyzed using a motion-compensating GLM [24] with a low statistical threshold ($T \geq 2.00$) to create a subject- and session-specific "activation mask." The first term of the GLM consisted of the modeled response, which was initially based on previous estimates of the SEEP response function [20]. By extracting the responses from each of the corresponding activation masks (again, across subjects and sessions), a new SEEP response was generated. Thus, the modeled response was improved in a data-driven, iterative fashion using continuously updated GLMs to form new activation masks and measure new responses.

2.4. Data analysis

2.4.1. General

Data analysis was performed on Windows-based PC workstations using custom software written in MatLab (The Mathworks, Natick, MA, USA). All spinal fMRI data were initially acquired in 2-mm contiguous sagittal slices to maximize rostral–caudal coverage, but were subsequently reformatted into 1-mm^3 voxels, resliced into axial segments based on a manually defined reference line along the anterior edge of the cord, and spatially normalized as previously described [33].

2.4.2. SEEP Response estimation

By implementing a slow event-related spinal fMRI paradigm, we were able, for the first time, to directly

measure the SEEP impulse response — in this case, following brief applications of 22°C cold thermal stimulation. However, given that the results will strongly depend on which voxel time courses are extracted, some a priori knowledge is required to separate "activated" from "non-activated" regions.

A previous study of the spinal cord BOLD response generated subject-specific activation masks, small regions for each subject (mean±SD = 43±12 mm^3), based on activity patterns in a block-designed task [23]. The implicit assumption in this method, however, is that the activated areas will remain constant across experiments and stimulus durations, without adaptation effects such as habituation or sensitization to repeated stimuli [34]. Therefore, given the very brief nature and relatively low intensity of the stimuli used in the present experiment, and the distinct possibility that event-related changes may evoke different activation patterns than block-designed paradigms, we attempted to apply a more data-driven approach that makes fewer a priori assumptions about which voxels to include in the event-related activation masks (i.e., voxels from which to measure a response).

In the present study, activation masks for the event-related data were created on an individual basis, based on the data from each session. For every event-related dataset, both the image data (Fig. 2A) and the GLM terms (Fig. 2B) were reordered on a subject-by-subject and slice-by-slice basis to form two time-locked peristimulus responses over the 56 acquired volumes. With the use of a previously reported estimate of the brain SEEP response function [20], hereafter referred to as the "canonical" SEEP response, a voxel-wise linear regression analysis was performed using the following GLM:

$$S(t) = \beta_1 A(t) + \beta_2 B(t) + \beta_3 C(t) + \beta_4 R1(t) + \beta_5 R2(t) + \beta_6 R3(t) + \varepsilon(t) \quad (1)$$

where S is the measured MR signal at a given time (t), β_i are the regression coefficients, A is the modeled response (based on the paradigm and the predicted SEEP response), B is a constant function, C is a linear ramp function, $R1$–$R3$ are the subject- and slice-specific RESPITE motion-compensation terms [24], and ε is the residual/error term (see Fig. 2B). In accordance with previously reported methods [35], an activation mask was constructed by first analyzing each dataset with a very low statistical threshold ($T \geq 2.00$, corresponding to an uncorrected $P \leq .025$) to exclude voxels with highly irregular or inconsistent responses. Then, anatomically defined region of interest (ROI) masks were generated for each subject [33] to identify and remove any signal changes beyond the C5–C8 spinal cord segments.

After generating the activation masks for each event-related session, the time-locked signal intensities were extracted and fit to the GLM described in Eq. (1). Motion confounds were then removed from the measured response in each active voxel, such that:

$$S_{corr}(t) = S(t) - \sum_{i=3}^{6} \beta_i F_i(t) \quad (2)$$

$$S_{corr}(t) = \sum_{i=1}^{2} \beta_i F_i(t) + \varepsilon(t) \quad (3)$$

where S_{corr} is the motion-corrected signal at a given time (t), S is the measured signal, β_i are the regression coefficients and F_i are the GLM basis functions (i=1 for the model time course, i=2 for the constant function and i=3,4,5,6 for the linear ramp and three RESPITE functions). Thus, the motion-corrected time courses were averaged across all voxels in the activation mask to determine the average response for each subject (data not shown) and the average response for the entire group.

The event-related datasets were then reanalyzed using the empirically derived SEEP impulse response function (as described above), to generate new activation masks and, in turn, extract new motion-corrected time courses in an iterative fashion. As new estimates of the SEEP time course were generated, correlation analyses were performed to compare them to the preceding estimate, as well as the canonical SEEP response, so that the process could be repeated until the empirical responses either converged or reached a predetermined cutoff point (correlation coefficient ≤0.2) that would indicate that they had deviated considerably from the initial canonical SEEP response.

As shown in Fig. 3, the empirical SEEP responses continued to change over subsequent iterations until the correlation cutoff was reached after six empirical estimates of the SEEP response. In total, each of the 30 event-related spinal fMRI datasets (10 subjects×3 sessions each) were analyzed with seven different GLMs — substituting the canonical or any of the six empirically derived SEEP responses as the first function in the basis set — to characterize the spinal cord SEEP response using a predominantly data-driven approach.

2.4.3. Independent component analysis

Independent component analysis (ICA) was performed on the individual SEEP responses (from each of the 10 subjects) in order to extract the main temporal features from the data in an exploratory manner, investigate intersubject differences in response shape and lag time, and assess any potential contributions from remaining structured noise. All ICA analyses were carried out using MatLab and the fastICA algorithm [36,37], which is freely available (http://www.cis.hut.fi/projects/ica/fastica/).

Before running the fastICA program, data were first constrained using the built-in principal component analysis (PCA) and the "lastEig" command to reduce the

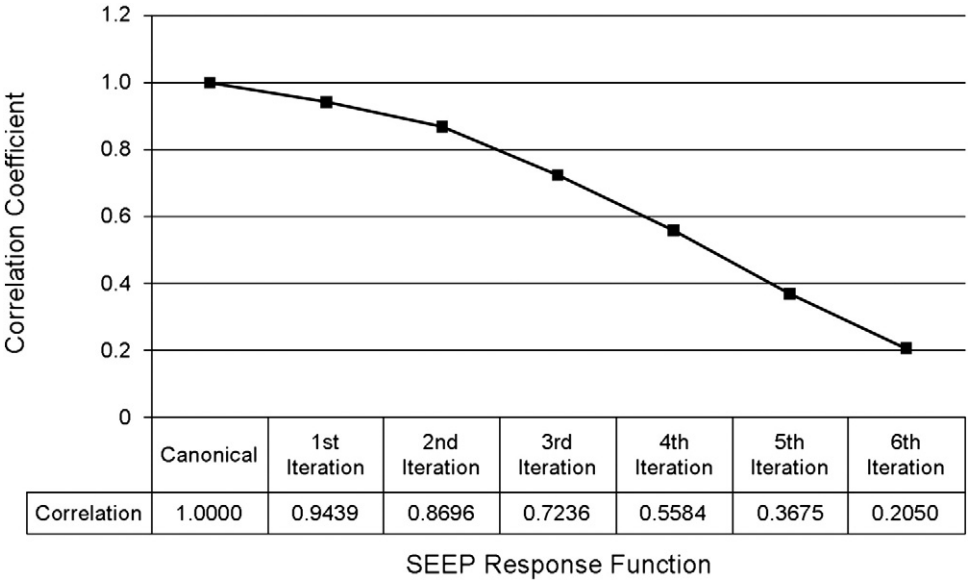

Fig. 3. Correlation of the empirically derived SEEP responses (shown in Fig. 5) to the previously described canonical SEEP response [20]. Correlations displayed a monotonic decrease that was roughly linear (slope=−0.0652) across the canonical, first iteration and second iteration. While the correlations of the latter responses also appeared to be linear, the correlation coefficients dropped off more than twice as sharply as the earlier iterations (slope=−0.1662). Based on this trend, the correlation coefficient of a subsequent iteration (0.0390) would be well below the predetermined cutoff value of 0.2.

dimensionality of the data along the two principal eigenvectors (corresponding to the response amplitude and peristimulus time). The fixed-point ICA algorithm was then run using a symmetric (as opposed to deflation) approach, to estimate the independent components in parallel. All other parameters, (e.g., the type of nonlinearity, convergence control, etc.) were left at the default values.

2.4.4. Random-effects analysis

Group analyses were performed on both the block-designed and event-related spinal fMRI results. For the block-designed data, a voxel-wise linear regression analysis was performed for each subject by using a motion-compensating GLM [24], as described in Eq. (1). The only difference between this analysis and the one shown in Fig. 2B was that the modeled time course, $A(t)$, was a boxcar stimulation paradigm convolved with the canonical SEEP response function. The data from each subject were then spatially normalized and coregistered to a standard spinal cord reference volume to allow cross-subject comparisons [33]. Data were masked to a ROI containing only the C5–C8 spinal cord segments (i.e., the same region used to determine the SEEP response), and active voxels in the remaining group were identified as those having $T \geq 3.25$, where $T = \frac{\text{mean } \beta_1}{\text{SEM } \beta_1}$ across all 10 subjects.

Group analyses of the event-related data were then carried out in a similar fashion to show areas of consistent event-related activity. For each subject, data were combined across all three event-related sessions to obtain a map of the average β_1 value for every voxel in the C5–C8 ROI. This was done for the canonical, as well as all six empirically measured SEEP responses. Group analyses were then performed for each iteration of the SEEP response using a statistical threshold of $T \geq 2.00$ across all 10 subjects. This threshold was chosen in order to achieve approximately the same amount of spinal cord activity (i.e., the number of active voxels) as the block-designed data analyzed at $T \geq 3.25$.

3. Results

3.1. SEEP Response estimation

SEEP signal-intensity changes were consistently identified during an event-related spinal fMRI paradigm consisting of 1-s applications of 22°C thermal stimulation. The empirically derived responses were then measured in an iterative fashion by extracting and averaging the motion-corrected time courses from the subject- and session-specific activation masks; namely, those voxels that where located within the C5–C8 spinal cord segments and identified using a GLM analysis with a low statistical threshold ($T \geq 2.00$).

A box plot showing the size of each activation mask is presented in Fig. 4, where the values in each row represent the number of voxels across all 30 event-related sessions (10 subjects×3 sessions) and each column represents a different iteration of the SEEP response. The gray bars denote the first and fourth quartiles (i.e., the lower and upper 25th percentiles), the white boxes denote the second and third quartiles (i.e., the middle 50th percentile), and the vertical lines at the interface of the second and third quartiles indicate the median number of voxels included in the activation mask for each response. As can be seen in the figure, the size of the activation masks increased rapidly

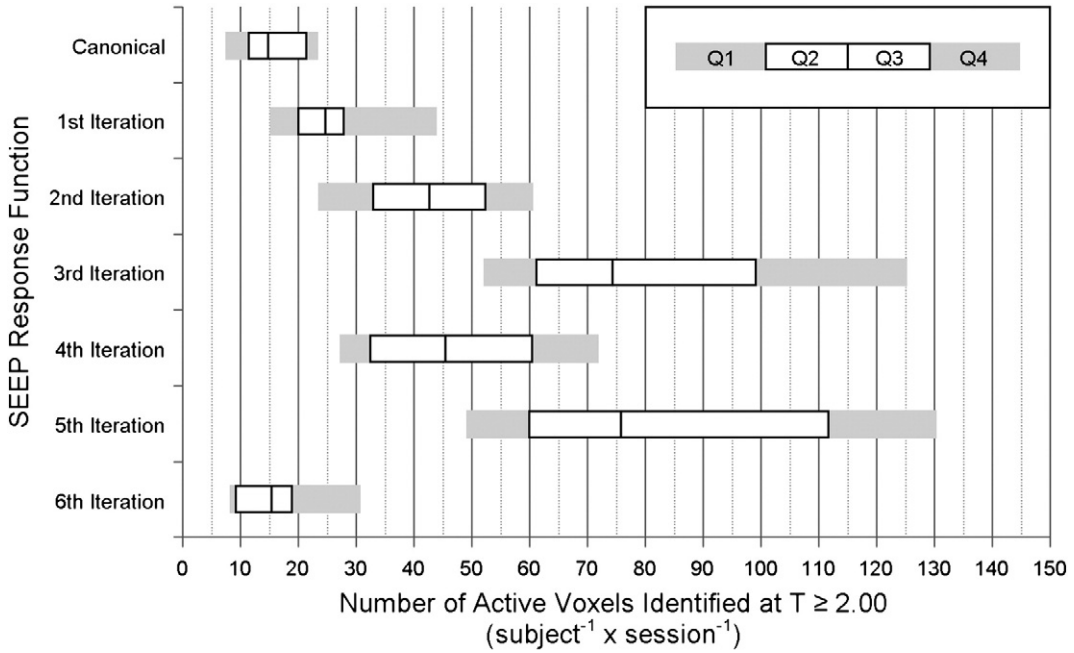

Fig. 4. Box plot showing the numerical distributions, in terms of the numbers of active voxels identified at $T \geq 2.00$ by each SEEP response (i.e., the size of the activation masks) in the event-related analyses. Distributions for each response are denoted by quartiles containing the lower and upper 25th percentiles (gray bars), as well as the median 50th percentile (white bars) transected by the median voxel count (vertical black line). The largest two activation masks were generated by the third and fifth iterations of the SEEP response ($P \leq .0001$).

for the first few iterations of the SEEP response, peaking at the third iteration, after which the sizes generally decreased (with the obvious exception of the fifth iteration). While the voxel counts for the third and fifth iterations of the SEEP response were statistically equivalent based on a paired two-tailed t test ($P=.40$), both of these generated significantly larger activation masks than any of the other responses ($P \leq .0001$).

For comparative purposes, it may be worth noting that activity detected from the block-designed data, analyzed with the canonical SEEP response, included far more voxels than any of the event-related data for any given session. For example, at the same statistical threshold used to create the event-related activation masks ($T \geq 2.00$), the smallest block-designed activation mask would have included 132 voxels — i.e., higher than even the largest event-related activation mask — with a median value of 214 and an interquartile range of 88 (data not shown). Greater statistical significance in the block-designed experiment, despite longer event-related sessions (8.7 min each vs. 6.9 min), implies that sustained periods of thermal stimulation may elicit larger and more distributed spinal cord responses than event-related stimuli of the same temperature, and suggests that using activation masks based on the block-designed data would have produced different overall results in terms of the measured SEEP responses.

Fig. 5 shows the canonical SEEP response, as well as the six experimentally derived SEEP time courses from the iterative analysis. The group averages were first smoothed with a three-point sliding window in order to minimize high-frequency fluctuations, and then intensity-normalized to facilitate direct comparisons between responses. The resulting surface plots, along with the values summarized in Table 1, show that, while the onset time (OT) and the time to peak (TTP) monotonically increased, the return to baseline (RTB) remained relatively constant, leading to decreased width of the response (full-width at half maximum, FWHM) in subsequent iterations. Also, despite the fact that the canonical SEEP response contained no negative values, both pre- and poststimulus undershoots appeared to emerge, particularly in the later iterations of the SEEP response. Please note that all response parameters in Table 1 (OT, TTP, RTB and FWHM) are defined in relation to the peristimulus time and are in units of seconds.

In order to investigate the main trends of the SEEP response and the sources of the apparent undershoots, ICA was performed on the average signal time courses from each subject. Using the activation mask generated from the canonical SEEP response and extracting the average time-locked signal intensity (i.e., the first iteration response) from each subject, Fig. 6 demonstrates that the response function was quite consistent, but not identical, across subjects. Furthermore, plotting the independent components from the fastICA analysis shows that the first independent component fits the group data very well, while the second independent component appears to be structured noise that could result from either a small number of outlying data points and/or residual physiological motion. Although the extracted time courses were motion compensated with RESPITE terms to minimize the effects of cardiac-related spinal cord motion, it

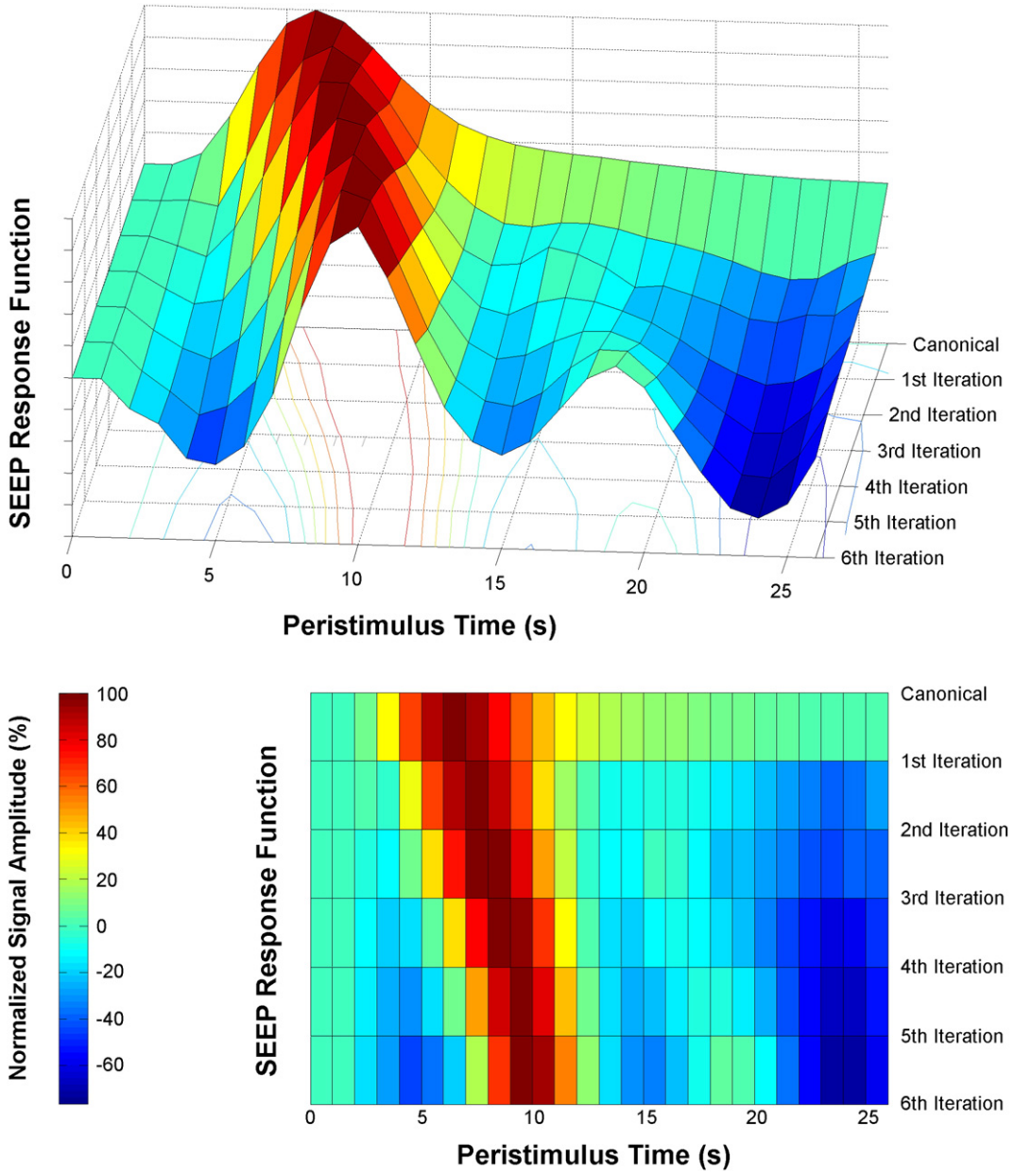

Fig. 5. Surface plots of the canonical SEEP response and the signal time courses of all six experimental iterations. Response amplitudes were normalized within each dataset, smoothed across three time points and then plotted in accordance with the color bar (lower left). The upper and lower panels show the same data from different vantage points to highlight the different features and trends of the responses. The upper panel clearly demonstrates the pre- and poststimulus undershoots that became apparent in the later iterations, as well as the delayed onset time of the response. The lower panel serves to highlight the increasing time to peak and decreasing response width (see also Table 1).

is possible that the entire second component, and perhaps even the small poststimulus undershoot in the first component, could result from residual contributions of structured physiological noise. Therefore, due to the iterative approach employed in this study, it is possible that subsequent analyses could propagate or even enhance these trends along with the actual impulse response. Considering that the individual responses and group ICA data in Fig. 6 do not strongly support the existence of pre- or poststimulus undershoots in the spinal cord SEEP response, undershoots emerging in subsequent iterations of the averaged responses (Fig. 5) may be artifactual.

3.2. Random-effects analysis

For the block-designed and event-related sessions, random-effects analyses were performed to identify consistent regions of activity across subjects (Fig. 7). Given that all stimuli were applied to the right thenar eminence, corresponding roughly to the C6 spinal cord segment, data were

Table 1
Quantitative parameters including onset time (OT), time to peak (TTP), return to baseline (RTB) and the full-width at half maximum (FWHM) for the canonical SEEP response, as well as each of the empirically derived SEEP responses

Response	OT	TTP	RTB	FWHM
Canonical	0	6.0	26.0	6.0
1	3.1	7.0	12.2	5.0
2	3.7	7.4	11.9	4.7
3	4.7	8.2	12.1	4.2
4	5.7	9.0	12.3	3.8
5	6.5	9.2	12.5	3.5
6	7.1	9.8	12.7	3.4

All values are reported in seconds and are relative to the peristimulus time (Fig. 5; x-axis). OT was defined as $f(x)=0$ with a positive slope; TTP was defined as $f(x)$=maximum; RTB was defined as $f(x)=0$ with a negative slope; FWHM was defined as the distance between the two points at $f(x)=1/2$ maximum.

masked on a subject-by-subject basis to include the C5–C8 spinal cord segments before performing the group analyses. Spinal fMRI data from the block-designed paradigm showed consistent regions of activity on the ipsilateral side of the C6 and C7 spinal cord segments, with uniform distributions of activity in the axial plane spanning several millimeters in the rostral–caudal dimension — and although more variable, similar patterns of activation also emerged for many of the event-related group analyses.

For the event-related data, the nominal sensitivity was observed to change depending on which SEEP response function was used to create the individual activation maps (Fig. 4), and although some regions were consistently observed regardless of the input SEEP response, the response function also affected the group T statistics (Fig. 7). In the event-related group activity maps, each response function identified a unique distribution of regions exceeding the statistical threshold ($T\geq 2.00$), with similar SEEP responses tending to generate similar statistical maps (Fig. 7). In general, earlier versions of the response (i.e., the first, second and third iterations) produced group activity patterns that were more like the block-designed and canonical event-related data than later versions of the response (i.e., the fourth, fifth and sixth iterations).

4. Discussion

4.1. General

To the best of our knowledge, this study represents the first successful demonstration of event-related spinal fMRI and the first characterization of the spinal cord SEEP response. These findings therefore show the high resolution (2.08-mm^3 voxels) and high degree of sensitivity that can be achieved with spinal fMRI methods using PD-

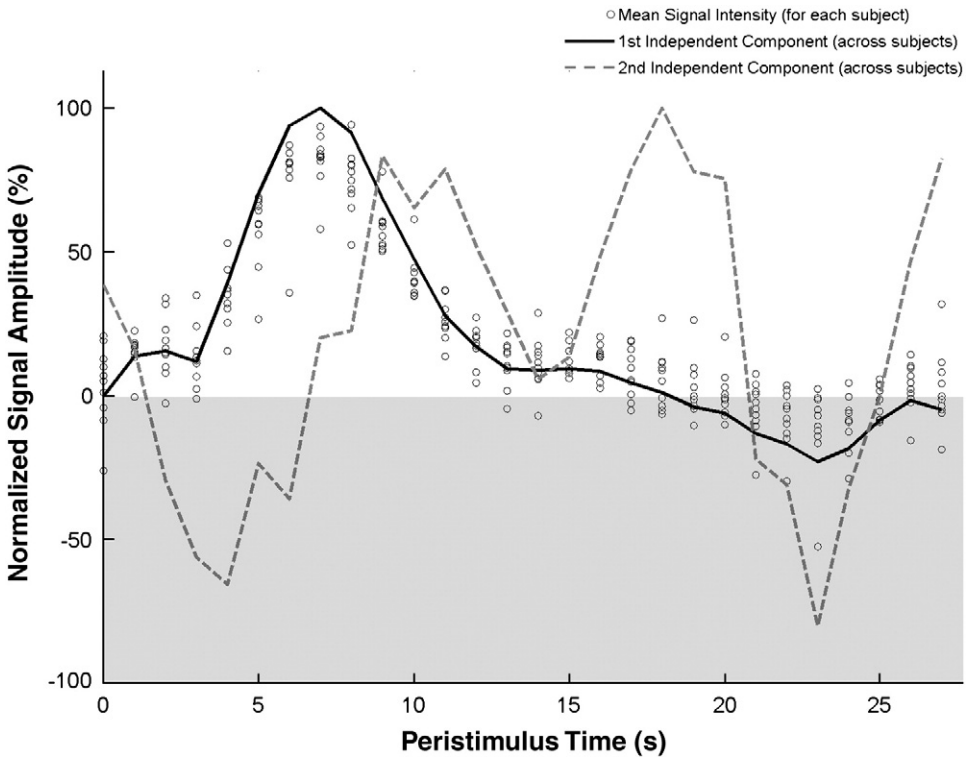

Fig. 6. Response time courses identified with the canonical activation mask to form the "first iteration." After fitting the raw extracted time courses with a GLM (Fig. 2) and removing the motion-related RESPITE confounds, the mean time-locked signal was generated separately for each subject (black circles). The first two independent components (solid and dashed lines) were then generated with the fastICA algorithm to identify the major trends of the SEEP response shape across all 10 subjects.

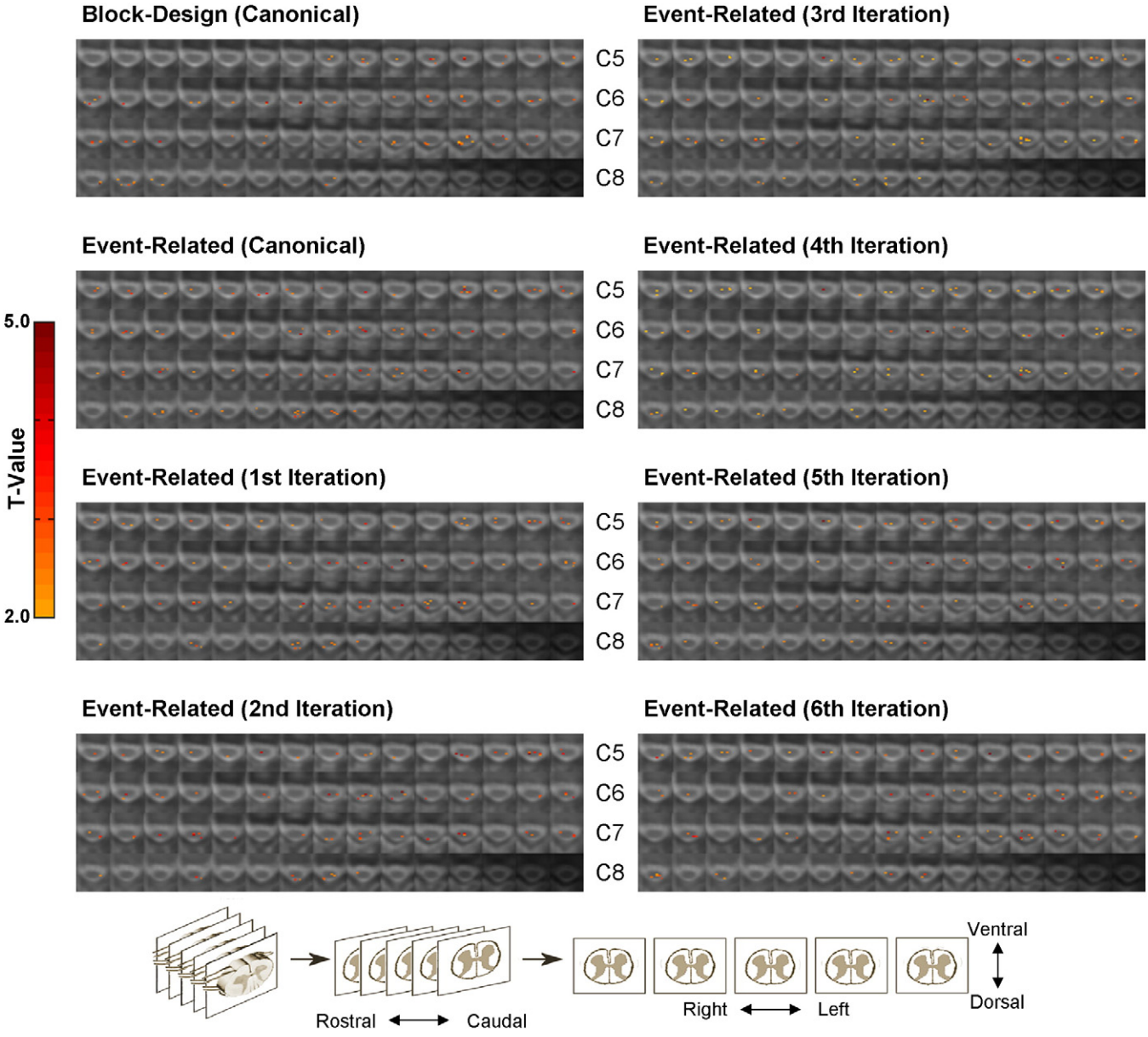

Fig. 7. Random-effects analyses of the block-designed and event-related data, showing consistent regions of activity across all 10 subjects ($T \geq 2.00$). While the block-designed data were analyzed using only the canonical SEEP response, the event-related data were analyzed separately with each of the seven SEEP time courses ("canonical" to "sixth iteration", as shown in parentheses). The block-designed data show consistent areas of activity throughout the ipsilateral dorsal horn (corresponding to the first relay points of the spinothalamic tract), as well as some ipsilateral and contralateral ventral horn activity spanning contiguous 1-mm-thick transverse slices. Similar areas of activity were also observed in the event-related datasets, with slight changes in location and statistical significance depending on which SEEP response was used in the GLM. However, in general, similar SEEP responses tended to produce similar event-related activity maps, with the "canonical" and first three response iterations identifying regions of activity that were more like the block-designed data (compared to the last three iterations).

weighted HASTE acquisition parameters and motion-compensating GLM analysis techniques.

One interesting feature of our data is that the different iterations of the SEEP response did not converge on a single preferred time course. In the early iterations, the activation masks grew steadily, identifying more "active" voxels as the measured SEEP response evolved (Fig. 4). However, it is somewhat peculiar that the response curves continued to change (Fig. 5) after the number of voxels in the activation masks dropped off — particularly since larger numbers of voxels might have been expected to dominate in their contribution to the average response time course. It is also interesting that the measured SEEP responses narrowed dramatically in subsequent iterations (Fig. 5 and Table 1), despite temporal smoothing of the response (using a three-point moving average) at each stage of the analysis.

4.2. Region of interest vs. functional activation masks

Since previous fMRI data have shown that only a small proportion of spinal cord voxels may be activated in any given task, and that these regions can be widely distributed both along the cord and throughout its cross-sectional area, choosing which voxels to include in the response time course is a difficult problem. During global hypercapnic challenge, BOLD increases have been reported to occur throughout ~35% of the brain, but less than 10% of the spinal cord, suggesting that spinal cord activity might be more localized [38]. Moreover, the magnitude and statistical significance of spinal cord BOLD responses has been shown to increase markedly (compared to hemicord ROI analyses) when values were averaged across only those voxels that were previously identified, with a GLM analysis, as preferentially responding to the stimuli [39]. This study found that when noxious and innocuous somatosensory stimuli were applied to the hand dorsum, only a small subset of the voxels in their original hemicord ROI were activated (15% and 8%, respectively). Furthermore, the authors showed that employing functional activation masks, similar to the approach used in the present study, improved the final response estimation and increased the mean spinal cord responses to noxious stimuli from ~1.5% (based on all of the voxels in their hemicord ROI) to ~3.5% (using only the selectively active voxels).

Nonetheless, one potential criticism of our method is that the SEEP response estimates may have been arrived at through circular logic: by applying functional activation masks and extracting time courses that were themselves based on an initial estimate of the SEEP response. However, in contrast, our data suggest that generating the activation masks with a liberal statistical threshold ($T \geq 2.00$) allowed the response shape to wander slowly (over multiple iterations) in a data-driven manner. This is supported by the fact that the activation masks extracted different response shapes both across iterations (Fig. 5) and across subjects within the same iteration (Fig. 6), implying that the chosen statistical threshold was low enough to allow the results to vary from our initial estimate (i.e., the canonical SEEP response), but stringent enough to filter out grossly erroneous responses.

4.3. Block-designed vs. event-related spinal fMRI results

By exploiting the sensitivity and reliability of state-of-the-art spinal fMRI methods, this study is the first to measure changes in spinal cord activity in response to very brief (i.e., 1 s) periods of stimuli. The SEEP responses were observed on an individual basis, showing good consistency across 10 subjects (Fig. 6), and statistical maps showing areas of group activity were generated for each iteration of the modeled SEEP time course (Fig. 7). While the block-designed data were more sensitive than the event-related data (identifying more active voxels at a given statistical threshold), random-effects analysis of the event-related data showed that regions of activity were routinely identified at the group level, and that, overall, these areas were consistent with the block-designed results.

Not surprisingly, the event-related maps depended to some degree on which iteration of the modeled SEEP response was employed in the analysis, with the earlier iterations more closely matching the block-designed results (Fig. 7). Based on this assessment, it appears that the optimal SEEP response for event-related spinal fMRI is likely somewhere between the canonical SEEP response and the second or third empirical iteration, and among these, the third iteration of the SEEP response had the highest nominal sensitivity, identifying the most statistically significant voxels per event-related dataset (Fig. 4). Therefore, based on a combination of sensitivity and visual comparison of the activation maps relative to the block-designed data (i.e., our best estimate for general location), we propose that the third iteration represents the optimal spinal cord SEEP response, with an estimated TTP of ~8.2 s and a FWHM of ~4.2 s (Fig. 5 and Table 1).

4.4. SEEP vs. BOLD response estimation in the cervical spinal cord

There is now a significant body of literature describing the BOLD hemodynamic response function, and it is well-known that both the magnitude and time course vary across subjects and brain regions [21,22,40]. BOLD responses have also been shown to depend on age [41,42]; disparities in vascular anatomy, arteriole supply, capillary perfusion and venous drainage [43]; blood hematocrit levels [44]; and ingestion of vasoactive substances such as alcohol [45], caffeine [46–50] or even excess lipids [51] prior to the experiment.

To date, T_2^*-weighted BOLD fMRI responses have been characterized in the cervical spinal cord during blocks of a bulb-squeezing motor task [23]. With a deconvolution approach, the optimal BOLD response in the spinal cord was estimated to have a TTP≈9.34 or 9.14 s and FWHM≈10.5 or 8.1 s, depending on whether the data were modeled with or without a poststimulus undershoot, respectively. These data suggest that the spinal cord BOLD response is much slower and wider compared to typically observed time courses in the brain, possibly owing to differences in vascular anatomy, cytoarchitecture and regional metabolism between the brain and spinal cord. For example, it has recently been shown that caudal brain regions exhibit reduced aerobic glycolysis compared to more rostral regions [52], so it is possible that these differences may extend into the spinal cord. However, since the spinal cord BOLD response was measured before the development of motion-compensating spinal fMRI methods [24,53], it is also possible that the estimated response contained components of cardiac or other physiological noise [25–27].

On the other hand, spinal cord SEEP responses measured in the present study had TTPs ranging from 6.0 to 9.8 s and corresponding FWHMs between 6.0 s and 3.4 s (Table 1),

with the optimum response estimated as having an 8-s TTP and a 4-s FWHM. Therefore, while SEEP responses are roughly 1 s slower than corresponding BOLD responses in the brain [20], it appears that SEEP signal changes in the spinal cord are faster and narrower compared to spinal cord BOLD responses. However, because the current study incorporated motion compensation and used short epochs of thermal stimulation to measure the SEEP impulse response function, it is possible that the differences between the spinal cord SEEP and BOLD responses resulted from a combination of the different biophysical mechanisms [16–19] and other experimental factors (e.g., task-related differences between sensory and motor processing).

Compared to previous SEEP response estimates in the brain [20], the time course in the spinal cord tended to be slower and narrower, and although apparent pre- and poststimulus undershoots emerged in later iterations (Fig. 5), visualization of the individual responses and the fastICA results (Fig. 6) suggests that these are not general features of the spinal cord SEEP response. While RESPITE terms were used to create the activation masks and to subtract the contributions of spinal cord motion from the measured responses, the apparent undershoots can likely be attributed to remaining sources of structured noise in the time-course data of a small number of subjects, as evidenced by the deviating responses and the second independent component shown in Fig. 6. Interestingly, the spinal cord BOLD response has also been shown to lack a poststimulus undershoot for stimulation periods shorter than 21 s, and even for longer blocks of stimulation, the amplitude of the undershoot was only ~11% relative to the peak response [23] (i.e., much lower than undershoot values in the brain, which can be as large as 50% [54]). Therefore, the lack of a poststimulus undershoot is consistent with previous SEEP response measurements in the brain [20] and spinal cord BOLD responses [23].

Overall, the fact that the SEEP responses were highly consistent across subjects suggests that the motion-compensation approach was generally effective in removing components of structured noise and implies that response variability across subjects was not likely a major concern for the random-effects analysis of our event-related spinal fMRI data (discussed above).

4.5. Implications for future event-related spinal fMRI studies

Our conclusion that the spinal cord SEEP response lacks a poststimulus undershoot is supported by previous SEEP response estimates in the brain [20] and fits with the proposed contrast mechanism based on changes in tissue water content [16–19]. However, the decision of whether or not to include a small undershoot in the response is not likely to be as critical for analyzing group results compared to accurately determining the other response parameters. For instance, small variations in OT and TTP have been shown to greatly influence statistical mapping in cross-subject analyses, whereas the inclusion or removal of poststimulus undershoots in modeled BOLD responses had relatively minor effects [21]. This also suggests that the variability of event-related activity maps in Fig. 7 (i.e., across SEEP responses) is likely attributable to changes in the OTs and TTPs, rather than to the emergence of the apparent, but likely erroneous, poststimulus undershoots.

Although spinal fMRI experiments have routinely identified functional responses during longer blocks of stimulation, previous experiments have failed to detect spinal cord activity during stimulation epochs shorter than 15 s [23]. Therefore, the relative success of the present study compared to earlier attempts of event-related spinal fMRI can likely be attributed to major differences in image acquisition and analysis methods. In terms of the image acquisition parameters, the previous study by Giulietti et al. [23] used T_2^*-weighted GE-EPI to measure BOLD signal changes at 1.5 T, while we used a PD-weighted HASTE sequence to measure the SEEP contrast at 3.0 T. Furthermore, because of the improved signal-to-noise ratio and reduced sensitivity to magnetic susceptibility artifacts (from the vertebrae and intervertebral disks), the present study was able to achieve better spatial resolution (2.08 vs. ~7.95 mm^3 overall, and 1.02 vs. 9.00 mm in the rostral–caudal dimension) in order to minimize the contribution of partial volume effects between active and inactive regions. As for analysis, all spinal fMRI data in our study were analyzed with a motion-compensating GLM [24], which has been shown to improve the sensitivity and specificity to activity-induced changes by modeling cardiac-related spinal cord motion [25–27].

Based on these findings, it seems that specialized acquisition and analysis methods (incorporating recent advances such as motion compensation) are extremely beneficial and may be necessary for future event-related spinal fMRI studies, while careful study design and the choice of stimuli will also play crucial roles. Although the current experiment employed widely spaced stimuli and a fixed ISI, these design features were only necessary so that the shape of the SEEP response could be directly measured and allowed to return to baseline between stimuli. However, now that the spinal cord SEEP response has been characterized, future spinal fMRI experiments should be able to achieve much higher design efficiencies by using rapid event-related approaches and jittered ISIs [55].

5. Conclusions

Using a predominantly PD-weighted HASTE sequence and motion-compensating GLM analyses to measure peristimulus responses throughout the human cervical spinal cord (i.e., 1-s applications of cold thermal stimulation), this study represents both the first successful event-related spinal fMRI experiment and the first thorough investigation of the

spinal cord SEEP response function. Our findings suggest that, compared to previous reports, the spinal cord SEEP response — with an OT, TTP, RTB and FWHM of approximately 5, 8, 12 and 4 s, respectively, and no clear evidence of a pre- or poststimulus undershoot — is approximately 1 s faster than the spinal cord BOLD response, 2 s slower than SEEP responses in the brain and several seconds slower than BOLD responses in the brain. While the current study deliberately implemented a slow event-related paradigm to measure the peristimulus SEEP response, our results suggest that similar imaging and analysis methods could be used to perform more rapid event-related spinal fMRI studies in the future.

Acknowledgments

We wish to thank Sharon David for technical support, as well as Teresa McAdam, Jordan Leitch, Chris Kidd, Rachael Bosma and Randi Beazer for helpful discussions and comments regarding preliminary drafts of the manuscript.

References

[1] Rosen BR, Buckner RL, Dale AM. Event-related functional MRI: past, present, and future. Proc Natl Acad Sci U S A 1998;95(3):773–80.
[2] Buckner RL, Bandettini PA, O'Craven KM, Savoy RL, Petersen SE, Raichle ME, et al. Detection of cortical activation during averaged single trials of a cognitive task using functional magnetic resonance imaging. Proc Natl Acad Sci U S A 1996;93(25):14878–83.
[3] McCarthy G, Luby M, Gore J, Goldman-Rakic P. Infrequent events transiently activate human prefrontal and parietal cortex as measured by functional MRI. J Neurophysiol 1997;77(3):1630–4.
[4] Friston KJ, Fletcher P, Josephs O, Holmes A, Rugg MD, Turner R. Event-related fMRI: characterizing differential responses. NeuroImage 1998;7(1):30–40.
[5] Curtis CE, D'Esposito M. Success and failure suppressing reflexive behavior. J Cogn Neurosci 2003;15(3):409–18.
[6] Stroman PW. Magnetic resonance imaging of neuronal function in the spinal cord: spinal FMRI. Clin Med Res 2005;3(3):146–56.
[7] Giove F, Garreffa G, Giulietti G, Mangia S, Colonnese C, Maraviglia B. Issues about the fMRI of the human spinal cord. Magn Reson Imaging 2004;22(10):1505–16.
[8] Leitch JK, Figley CR, Stroman PW. Applying functional MRI to the spinal cord and brainstem. Magn Reson Imaging 2010;28(8):1225–33.
[9] Summers PE, Iannetti GD, Porro CA. Functional exploration of the human spinal cord during voluntary movement and somatosensory stimulation. Magn Reson Imaging 2010;28(8):1216–24.
[10] Bouwman CJ, Wilmink JT, Mess WH, Backes WH. Spinal cord functional MRI at 3 T: gradient echo echo-planar imaging versus turbo spin echo. NeuroImage 2008;43(2):288–96.
[11] Stroman PW, Kornelsen J, Lawrence J. An improved method for spinal functional MRI with large volume coverage of the spinal cord. J Magn Reson Imaging 2005;21(5):520–6.
[12] Stroman PW. Discrimination of errors from neuronal activity in functional MRI of the human spinal cord by means of general linear model analysis. Magn Reson Med 2006;56(2):452–6.
[13] Ogawa S, Lee TM, Kay AR, Tank DW. Brain magnetic resonance imaging with contrast dependent on blood oxygenation. Proc Natl Acad Sci U S A 1990;87(24):9868–72.
[14] Ogawa S, Lee TM, Nayak AS, Glynn P. Oxygenation-sensitive contrast in magnetic resonance image of rodent brain at high magnetic fields. Magn Reson Med 1990;14(1):68–78.
[15] Ogawa S, Tank DW, Menon R, Ellermann JM, Kim SG, Merkle H, et al. Intrinsic signal changes accompanying sensory stimulation: functional brain mapping with magnetic resonance imaging. Proc Natl Acad Sci U S A 1992;89(13):5951–5.
[16] Stroman PW, Lee AS, Pitchers KK, Andrew RD. Magnetic resonance imaging of neuronal and glial swelling as an indicator of function in cerebral tissue slices. Magn Reson Med 2008;59(4):700–6.
[17] Stroman PW, Krause V, Malisza KL, Frankenstein UN, Tomanek B. Extravascular proton-density changes as a non-BOLD component of contrast in fMRI of the human spinal cord. Magn Reson Med 2002;48 (1):122–7.
[18] Figley CR, Leitch JK, Stroman PW. In contrast to BOLD: signal enhancement by extravascular water protons as an alternative mechanism of endogenous fMRI signal change. Magn Reson Imaging 2010;28(8):1234–43.
[19] Figley CR, Stroman PW. The role(s) of astrocytes and astrocyte activity in neurometabolism, neurovascular coupling, and the production of functional neuroimaging signals. Eur J Neurosci 2011;33(4): 577–88.
[20] Stroman PW, Kornelsen J, Lawrence J, Malisza KL. Functional magnetic resonance imaging based on SEEP contrast: response function and anatomical specificity. Magn Reson Imaging 2005;23 (8):843–50.
[21] Handwerker DA, Ollinger JM, D'Esposito M. Variation of BOLD hemodynamic responses across subjects and brain regions and their effects on statistical analyses. NeuroImage 2004;21(4):1639–51.
[22] Huettel SA, McCarthy G. Regional differences in the refractory period of the hemodynamic response: an event-related fMRI study. NeuroImage 2001;14(5):967–76.
[23] Giulietti G, Giove F, Garreffa G, Colonnese C, Mangia S, Maraviglia B. Characterization of the functional response in the human spinal cord: Impulse-response function and linearity. NeuroImage 2008;42 (2):626–34.
[24] Figley CR, Stroman PW. Development and validation of retrospective spinal cord motion time-course estimates (RESPITE) for spin-echo spinal fMRI: improved sensitivity and specificity by means of a motion-compensating general linear model analysis. NeuroImage 2009;44(2):421–7.
[25] Figley CR, Stroman PW. Investigation of human cervical and upper thoracic spinal cord motion: implications for imaging spinal cord structure and function. Magn Reson Med 2007;58(1):185–9.
[26] Figley CR, Yau D, Stroman PW. Attenuation of lower-thoracic, lumbar, and sacral spinal cord motion: implications for imaging human spinal cord structure and function. AJNR Am J Neuroradiol 2008;29 (8):1450–4.
[27] Piche M, Cohen-Adad J, Nejad MK, Perlbarg V, Xie G, Beaudoin G, et al. Characterization of cardiac-related noise in fMRI of the cervical spinal cord. Magn Reson Imaging 2009;27(3):300–10.
[28] Stroman PW. Spinal fMRI investigation of human spinal cord function over a range of innocuous thermal sensory stimuli and study-related emotional influences. Magn Reson Imaging 2009;27(10):1333–46.
[29] Ghazni NF, Cahill CM, Stroman PW. Tactile sensory and pain networks in the human spinal cord and brain stem mapped by means of functional MR imaging. AJNR Am J Neuroradiol 2010;31(4):661–7.
[30] Dykest RW, Terzis JK. Spinal nerve distributions in the upper limb: the organization of the dermatome and afferent myotome. Phil Trans R Soc Lond B 1981;293(1070):509–54.
[31] Stroman PW, Krause V, Malisza KL, Frankenstein UN, Tomanek B. Functional magnetic resonance imaging of the human cervical spinal cord with stimulation of different sensory dermatomes. Magn Reson Imaging 2002;20(1):1–6.
[32] Josephs O, Turner R, Friston KJ. Event-related fMRI. Hum Brain Mapp 1997:5243–8.
[33] Stroman PW, Figley CR, Cahill CM. Spatial normalization, bulk motion correction and coregistration for functional magnetic resonance imaging of the human cervical spinal cord and brainstem. Magn Reson Imaging 2008;26(6):809–14.

[34] Krekelberg B, Boynton GM, van Wezel RJ. Adaptation: from single cells to BOLD signals. Trends Neurosci 2006;29(5):250–6.
[35] Glover GH. Deconvolution of impulse response in event-related BOLD fMRI. NeuroImage 1999;9(4):416–29.
[36] Bingham E, Hyvarinen A. A fast fixed-point algorithm for independent component analysis of complex valued signals. Int J Neural Syst 2000;10(1):1–8.
[37] Hyvärinen A, Oja E. A fast fixed-point algorithm for independent component analysis. Neural Comput 1997;9(7):1483–92.
[38] Cohen-Adad J, Gauthier CJ, Brooks JC, Slessarev M, Han J, Fisher JA, et al. BOLD signal responses to controlled hypercapnia in human spinal cord. NeuroImage 2010;50(3):1074–84.
[39] Summers PE, Ferraro D, Duzzi D, Lui F, Iannetti GD, Porro CA. A quantitative comparison of BOLD fMRI responses to noxious and innocuous stimuli in the human spinal cord. NeuroImage 2010;50(4): 1408–15.
[40] Aguirre GK, Zarahn E, D'Esposito M. The variability of human, BOLD hemodynamic responses. NeuroImage 1998;8(4):360–9.
[41] D'Esposito M, Zarahn E, Aguirre GK, Rypma B. The effect of normal aging on the coupling of neural activity to the bold hemodynamic response. NeuroImage 1999;10(1):6–14.
[42] Huettel SA, Singerman JD, McCarthy G. The effects of aging upon the hemodynamic response measured by functional MRI. NeuroImage 2001;13(1):161–75.
[43] Carusone LM, Srinivasan J, Gitelman DR, Mesulam MM, Parrish TB. Hemodynamic response changes in cerebrovascular disease: implications for functional MR imaging. AJNR Am J Neuroradiol 2002;23(7): 1222–8.
[44] Levin JM, Frederick BB, Ross MH, Fox JF, von Rosenberg HL, Kaufman MJ, et al. Influence of baseline hematocrit and hemodilution on BOLD fMRI activation. Magn Reson Imaging 2001;19(8): 1055–62.
[45] Levin JM, Ross MH, Mendelson JH, Kaufman MJ, Lange N, Maas LC, et al. Reduction in BOLD fMRI response to primary visual stimulation following alcohol ingestion. Psychiatry Res 1998;82(3): 135–46.
[46] Chen Y, Parrish TB. Caffeine's effects on cerebrovascular reactivity and coupling between cerebral blood flow and oxygen metabolism. NeuroImage 2009;44(3):647–52.
[47] Chen Y, Parrish TB. Caffeine dose effect on activation-induced BOLD and CBF responses. NeuroImage 2009;46(3):577–83.
[48] Mulderink TA, Gitelman DR, Mesulam MM, Parrish TB. On the use of caffeine as a contrast booster for BOLD fMRI studies. NeuroImage 2002;15(1):37–44.
[49] Laurienti PJ, Field AS, Burdette JH, Maldjian JA, Yen YF, Moody DM. Dietary caffeine consumption modulates fMRI measures. NeuroImage 2002;17(2):751–7.
[50] Liu TT, Behzadi Y, Restom K, Uludag K, Lu K, Buracas GT, et al. Caffeine alters the temporal dynamics of the visual BOLD response. NeuroImage 2004;23(4):1402–13.
[51] Noseworthy MD, Alfonsi J, Bells S. Attenuation of brain BOLD response following lipid ingestion. Hum Brain Mapp 2003;20(2): 116–21.
[52] Vaishnavi SN, Vlassenko AG, Rundle MM, Snyder AZ, Mintun MA, Raichle ME. Regional aerobic glycolysis in the human brain. Proc Natl Acad Sci U S A 2010;107(41):17757–62.
[53] Brooks JC, Beckmann CF, Miller KL, Wise RG, Porro CA, Tracey I, et al. Physiological noise modelling for spinal functional magnetic resonance imaging studies. NeuroImage 2008;39(2): 680–92.
[54] Chen JJ, Pike GB. Origins of the BOLD post-stimulus undershoot. NeuroImage 2009;46(3):559–68.
[55] Dale AM. Optimal experimental design for event-related fMRI. Hum Brain Mapp 1999;8(2–3):109–14.